Fickian Non-Gaussian Diffusion in Glass-Forming Liquids

Francesco Rusciano⬤, Raffaele Pastore⬤,[*] and Francesco Greco
Department of Chemical, Materials and Production Engineering, University of Naples Federico II,
Piazzale Tecchio 80, Napoli 80125, Italy

Fickian yet non-Gaussian diffusion (FnGD), a most intriguing open issue in soft matter, is generically associated with some dynamical and/or structural heterogeneity of the environment. Here we investigate the features of FnGD in glass-forming liquids, the epitome of dynamical heterogeneity, drawing on experiments on hard-sphere colloidal suspensions and simulations of a simple model of molecular liquid. We demonstrate that FnGD strengthens on approaching the glass transition, by identifying distinct timescales for Fickianity, τ_F, and for restoring of Gaussianity, $\tau_G > \tau_F$, as well as their associated length scales, ξ_F and ξ_G. We find $\tau_G \propto \tau_F^\gamma$ with $\gamma \simeq 1.8$ for both systems. In the deep FnGD regime, the displacement distributions display exponential tails. We show that, in simulations, the time-dependent decay lengths $l(t)$ at different temperatures all collapse onto a power-law master curve $[l(t)/(\xi_G)] \propto (t/\tau_G)^\alpha$, with $\alpha = 0.33$. A similar collapse, if less sharp, is also found in experiments, seemingly with the same exponent α. We further discuss the connections of the timescales and length scales characterizing FnGD with structural relaxation and dynamic heterogeneity.

According to Einstein's work on Brownian motion [1], macroscopic diffusion at equilibrium corresponds to random walks of thermally agitated particles, with a *Gaussian* displacement distribution, *plus* a mean square displacement (MSD), $\langle r^2(t) \rangle$, increasing linearly with time, the so-termed *Fickian* case: the diffusion constant is then obtained as $D = \langle r^2(t) \rangle / 2dt$, d being the space dimensionality. In more recent years, a variety of experiments has also shown the existence of anomalous (non-Fickian) diffusion, quite often associated with correlated walks, and typically accompanied by non-Gaussian displacement distributions [2,3]. Thus, from this double perspective, Fickian and Gaussian behaviors were thought to be biunivocally related.

In 2009, ground-breaking experiments [4] on nanometric beads in complex biological fluids broke up such a scenario, revealing the existence of a novel type of diffusion that is distinct from both standard and anomalous diffusion, being simultaneously Fickian *and* non-Gaussian. In the past few years, many other examples of such a "Fickian yet non-Gaussian diffusion" (FnGD) have been reported, mostly in soft matter and biological systems characterized by some kind of heterogeneity of the structure or in the dynamics [4–13]. The existence of an underlying heterogeneity has also been considered in various theoretical models [14–18] proposed to capture the main features of FnGD such as, for example, the presence of "fat tails" ("fatter than Gaussian," usually exponential) in the displacement distribution. While a full understanding of FnGD is still far from being achieved, the association between FnGD and some kind of heterogeneity generally meets a wide consensus [14,19,20].

Dealing with dynamical heterogeneity (DH), it comes naturally to think next of glass-forming liquids.

Single-particle dynamics in supercooled conditions is characterized by an intermittent motion, with a continuous alternation of localized vibrations inside the "cage" created by the surrounding particles, and sudden "jumps" to other cages [21–23]; on sufficiently large length scales and timescales, this leads to a grouping of "fast" and "slow" particles, the more so the more the glass transition is approached [24]. Thus, supercooled liquids are commonly considered the epitome of DHs. It is tempting to believe that they may also represent a paradigmatic example of FnGD.

Concerning the MSD in glass-forming liquids, it is well known that the long-time Fickian behavior is always preceded by a distinctive subdiffusive (or plateau) regime. Noticeably, exponentially tailed displacement distributions have been reported for both experiments on colloidal systems and molecular dynamic simulations [21,23,25] focusing on times of the order of the structural relaxation time τ_α, related to the first jumps of the particles out of their cages, which typically falls either within the subdiffusive regime or around the subdiffusive-Fickian crossover. Deviations from Gaussianity, however, can persist even in the Fickian regime [26], corresponding to timescales and length scales where, on average, particles have performed many jumps.

Overall, several pieces of the puzzle now suggest that FnGD could be a typical feature of glass-forming liquids, but this point has not been directly addressed so far [27]. In this Letter, we demonstrate that, on approaching glass transition, FnGD becomes more and more marked, and identify the scaling relations for its characteristic times and lengths. Further, we show the relevance of these characteristic scales in interpreting structural relaxation and dynamic heterogeneity in glass formers.
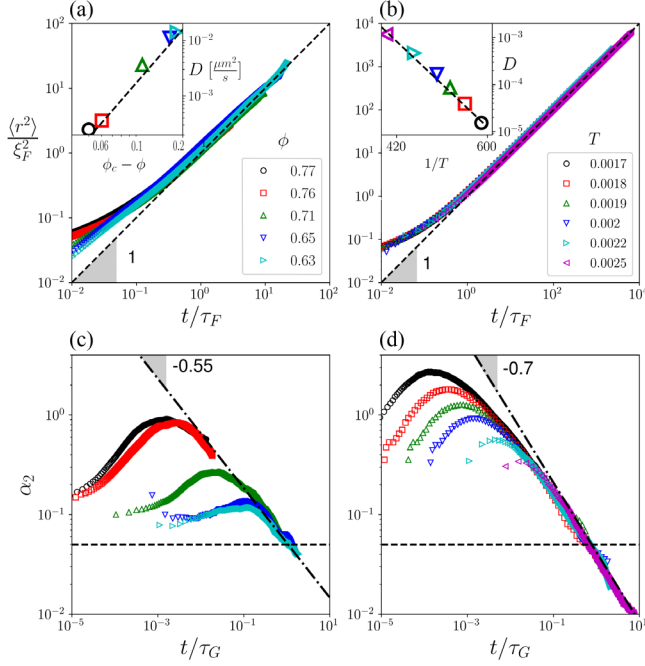
168001-1

FIG. 1.   (a) $\langle r^2 \rangle / \xi_F^2$ as a function of t/τ_F, for experiments at different area fractions. Dashed line indicates the Fickian behavior. Inset: diffusion coefficient as a function of area fraction. The dashed line is an MCT-like fit, $D \propto (\phi_c - \phi)^{b_D}$, with $\phi_c = 0.81 \pm 0.02$, $b_D = 2.8 \pm 0.2$. (b) Same quantities as in panel (a), for simulations at different temperatures expressed in MD units of the interparticle interaction energy scale ϵ (see Supplemental Material [29]). The dashed line in the inset is an Arrhenius fit, $D \propto e^{E_D/T}$, with $E_D = -0.0233 \pm 0.003$. Bottom panels: NGP as a function of t/τ_G for experiments (c) and simulations (d). The dashed lines indicate power laws with exponents -0.55 ± 0.15 and -0.7 ± 0.1, respectively. Unless otherwise specified, colors and symbols are the same in the following figures.

Our study draws on a combination of experiments and molecular dynamics (MD) simulations in equilibrium conditions (see Supplemental Material [29]). The experimental system is a suspension, at nearly monolayer conditions, of hard-sphere colloidal beads in water, where the dynamic slowdown is driven by increasing the area fraction ϕ [48–51]. The simulated system is a simple molecular liquid model, consisting of a 2D assembly of soft disks, where the dynamics slows down on decreasing the temperature T [22,52]. Both systems are quite popular two-dimensional glass-forming models and present qualitatively similar dynamical features on approaching the glass transition [53].

Figures 1(a) and 1(b) show, for experiments and simulations, MSDs as a function of time after rescaling of the axes for the Fickian timescales and length scales, τ_F and ξ_F. The adopted shifting factor are $\xi_F = \sigma$ and $\tau_F = [\sigma^2/(4D)]$ (see Supplemental Material [29]), where σ is the particle diameter. Hence, the Fickian length is constant, while the Fickian time, τ_F, which is also an estimate of the duration of subdiffusion, scales as the inverse of the diffusion

coefficient (see the insets of Fig. 1) on approaching the glass transition. The plot of $\langle r^2 \rangle / \xi_F^2$ versus t/τ_F demonstrates how effective is our identification of the Fickian timescales and length scales: indeed, all MSD datasets collapse on a linear master curve starting from the point of coordinates (1,1).

The approach used to identify the Gaussian timescale τ_G and the associated length scale $\xi_G = (4D\tau_G)^{1/2}$ is illustrated in Figs. 1(c) and 1(d), for experiments and simulations, respectively. We define τ_G as the time at which the non-Gaussian parameter (NGP) $\alpha_2(t)$ (see Supplemental Material [29]) reaches an arbitrarily chosen (low) threshold of 0.05. With this choice, the displacement distribution for $t \geq \tau_G$ is indistinguishable from the Gaussian distribution of standard Brownian motion.

By plotting the NGPs as a function of t/τ_G, we succeed in collapsing all the long-time tails over a well-defined master curve, a power law with exponent -0.55 for experiments and -0.7 for simulations (see Supplemental Material [29]). At high-ϕ/low-T conditions, where the adopted low threshold for α_2 is not attained within the monitored time, we estimate τ_G as the appropriate shifting factor to obtain the aforementioned data collapse. Notice that the existence of the data collapse ensures that the choice of the threshold does not affect the area fraction or temperature dependence of the estimated τ_G. Indeed, on changing the threshold, τ_G would merely change by a constant factor.

Figures 2(a) and 2(b) show the area fraction and temperature dependence of τ_F and τ_G, as measured through the just described approach, for experiments and simulations. For each system, the two timescales are well fitted by the same functional form: a power law $A(\phi_c - \phi)^b$ (with a unique $\phi_c = 0.81$) for experiments, and an Arrhenius law $Be^{(E/T)}$ for simulations. In both systems, τ_G is always larger and increases faster than τ_F on approaching the glass transition, as indicated by the power-law exponents (in experiments) and the activation energies (in simulations) of τ_G being roughly twice those estimated for τ_F. The just presented behavior implies that the two timescales are directly connected by a power-law relation, $\tau_G \propto \tau_F^\gamma$. In fact, a unique value of the exponent, $\gamma = 1.8$, is found for both experiments and simulations, as shown in the insets of panels (a) and (b).

Figures 2(c) and 2(d) show that the Gaussian length ξ_G grows on approaching the glass transition. As it can be directly inferred by the fits to D (see Fig. 1) and τ_G (see Fig. 2), the increase of ξ_G is well described by $\xi_G \propto (\phi_c - \phi)^{[(b_G - b_F)/2]}$ for experiments and $\xi_G \propto e^{[(E_G - E_D)/2]}$ for simulations. Overall, Fig. 2 clearly demonstrates that FnGD exists in both the examined systems, and spans increasingly larger timescales and length scales on approaching the glass transition.

Figures 3(a) and 3(b) show the displacement distributions $p(x,t)$ [54] at two representative values $\phi = 0.77$ and $T = 1.8 \times 10^{-3}$, for experiments and simulations,
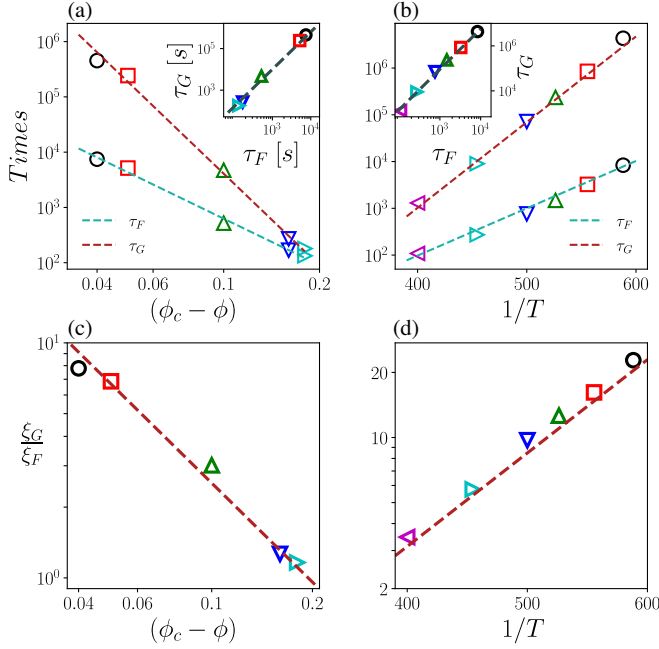
FIG. 2. τ_G and τ_F for experiments as a function of $(\phi_c - \phi)$ (a), and for simulations as a function of $1/T$ (b). Dashed lines in panel (a) are fits through power laws of $(\phi_c - \phi)$, with exponent $b_F = -b_D = -2.8 \pm 0.2$ for τ_F and $b_G = -5.5 \pm 0.2$ for τ_G, and with a unique $\phi_c = 0.81 \pm 0.01$. Dashed lines in panel (b) are Arrhenius fits $e^{(E/T)}$ with $E_F = -E_D = 2.3 \times 10^{-2} \pm 3 \times 10^{-3}$ for τ_F and $E_G = 4.2 \times 10^{-2} \pm 3 \times 10^{-3}$ for τ_G. Insets in panels (a) and (b) show scatter plots of τ_F vs τ_G. Dashed lines are power laws $\tau_G \propto \tau_F^{\gamma}$ with $\gamma = 1.8 \pm 0.2$. (c) and (d) ξ_G/ξ_F as a function of $(\phi_c - \phi)$ for experiments, and of $1/T$ for simulations. Dashed line in panel (c) is a power law $\xi_G \propto (\phi_c - \phi)^{[(b_G - b_F)/2]}$. Dashed line in panel (d) is an Arrhenius law $\xi_G \propto e^{[(E_G - E_F)/2T]}$.

respectively, and for many nondimensional times t/τ_G with $t > \tau_F$, i.e., within the FnGD regime. To properly compare the distributions at different times, we have rescaled the axes as follows: $x \to X = [x/(\sqrt{\langle x^2(t)\rangle})]$, and $p(x,t) \to P(X,t) = p(x,t)\sqrt{\langle x^2(t)\rangle}$, thus preserving normalization. It is worth noticing that the standard Gaussian distribution $g(x,t) = [(e^{-[x^2/(4Dt)]})/\sqrt{4\pi Dt}]$ becomes, after this rescaling, a universal time-independent master curve: $G(X) = \sqrt{(2/\pi)}e^{-(X^2/2)}$. Let us now separately discuss the two investigated systems. It proves convenient here to start from simulations.

The distributions in Fig. 3(b) always display an excess probability with respect to $G(X)$ both at small and large values of X, "compensated" by a defect probability at intermediate displacements. At large displacements and short times ($t/\tau_G < 0.1$), tails are well fitted by exponential decays $\simeq e^{-[(X)/L(t)]}$ over at least two orders of magnitude of probability values; the nondimensional decay length L shows a continuous decrease within this time range. Such an initial smooth change in L is then followed by the restoring of Gaussianity for the distribution function, which
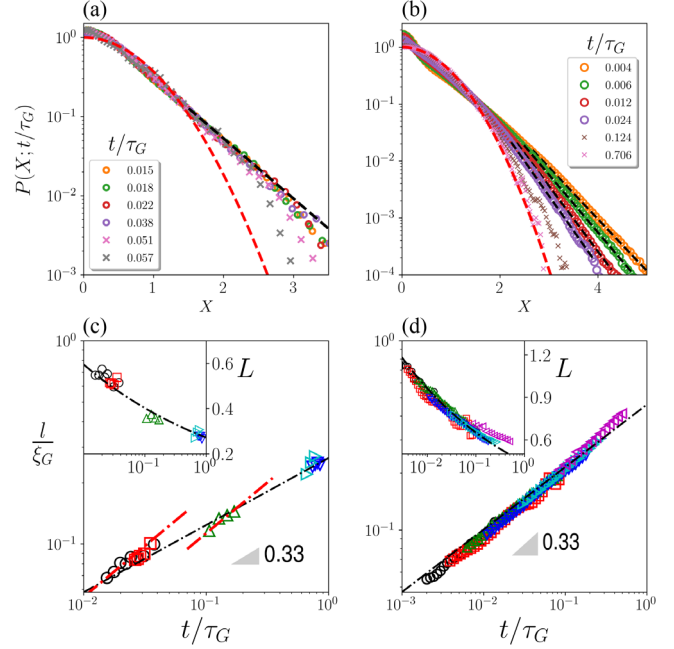

FIG. 3. $P(X, t/\tau_G)$ at different times within the FnGD regime (a) for experiments at $\phi = 0.77$, and (b) for simulations at $T = 1.8 \times 10^{-3}$. The red dashed lines are the universal Gaussian distribution $G(X)$. Empty circles cover the range of t/τ_G, where the distribution tails are reliably fitted by exponential decays. (c) and (d) The decay length $l(t)/\xi_G$ as function of t/τ_G, for experiments at different area fractions and for simulations at different temperatures, respectively. The black dashed line is a power law $l(t) \propto t^{0.33}$. Red dashed lines are $\propto t^{0.5}$ The insets show $L = l(t)/\sqrt{\langle x^2(t)\rangle}$ as a function of t/τ_G; the dashed line is a power law $L \propto t^{-0.17}$.

is fully attained in this example, consistently with the simulation time eventually reaching the estimated τ_G at this temperature ($\tau_G \approx 8 \times 10^5$).

Figure 3(d) shows $L(t/\tau_G)$ (inset) in the FnGD regime at all temperatures, in the time-range where exponential fits to the tails are reliable, together with the corresponding dimensional length $l = L\sqrt{4Dt}$ (main panel) commonly reported in literature on FnGD [4,5,7]. L data at all temperatures do collapse onto a power-law decrease:

$$L = C\left(\frac{t}{\tau_G}\right)^{-\zeta}, \tag{1}$$

C being a unique constant and $\zeta = 0.17 \pm 0.02$. Some deviations from this collapse are only observed at the highest temperature and large time, where, however, the fits to the distribution tails are less robust [55]. The occurrence of this master curve not only points out the power-law dependence of L upon time t/τ_G, but also highlights that the effect of changing temperature is fully captured by the T dependence of τ_G. Notice that the first point in each dataset in Fig. 3(d) corresponds to the ratio τ_F/τ_G as its abscissa.

Since such ratio decreases on lowering the temperature [see Fig. 2(b)], $L(\tau_F/\tau_G)$ is larger at lower temperatures, i.e., the exponential tails are more extended. In other words, on approaching the glass transition, FnGD becomes not only more time persistent, but also more marked. The just found behavior for L implies that, at any temperature, the dimensional decay length l increases as a power law of time with an exponent $\alpha = 0.5 - \zeta = 0.33 \pm 0.02$, which is different from the value 0.5 commonly reported in FnGD [4,5,7]. In addition, from Eq. (1), data corresponding to different temperatures will of course collapse onto a single power law, when plotted as $l(t)/\xi_G$ versus t/τ_G [see main Fig. 3(d)].

We now turn to experimental distributions, as the ones shown in Fig. 3(a). Seemingly, here, at small t/τ_G, the tails of the distributions nearly collapse onto an exponential decay with a unique L; for larger t/τ_G, evolution toward the Gaussian master curve is observed. Full restoring of Gaussianity is, however, far from being attained here, consistently with the fact that the estimated $\tau_G \approx 5 \times 10^5$ s at this area fraction is significantly larger than the total observation time $t = 3 \times 10^4$ s. At lower area fractions, we find the same qualitative scenario, with less persistent and weaker deviations from $G(X)$, consistently with the behavior of the NGP [Figs. 1(c) and 1(d)].

A comparison of Figs. 3(a) and 3(b) may suggest a different behavior of the exponential decay length, with $L \simeq$ const for experiments, but depending on time in simulations [see Eq. (1)]. Such difference should be carefully reconsidered, however, in the light of the relatively narrow ranges of times and probability available for the colloidal system. Indeed, in our experiments, t/τ_G for each concentration spans less than a decade, and probabilities are reliable down to 10^{-3}, at most. In simulations, by contrast, the range of t/τ_G for each temperature exceeds two decades, and probabilities are fairly well sampled down to 10^{-4}. Thus, our observation of a nearly constant L may simply be due to limited experimental data. As a matter of fact, experimental data for L and l/ξ_G as functions of t/τ_G, reported in Fig. 3(c), display collapses and scaling exponents that are compatible (at least) with those found in simulations [see Fig. 3(d)] [56]. However, the limited experimental datasets leave open the possibility that these scalings may be system dependent, as suggested in a recent study [28]. In this perspective, we notice that, at a single area fraction, data can be described equally well by "local fits" with exponents $\alpha = 0.33$ or $\alpha = 0.5$ (for local fits with $\alpha = 0.5$ at $\phi = 0.71$ and 0.77 see the red dot-dashed lines in Fig. 3(c); see also Supplemental Material [29]), but a "global fit," i.e., for all area fractions, with this latter power law will patently fail, at variance with what is found for the exponent $\alpha = 0.33$.

To have a complementary perspective on FnGD, we probe the dynamics through the intermediate self-scattering function (ISSF) $F_s(\lambda, t)$ at different wavelengths λ (see
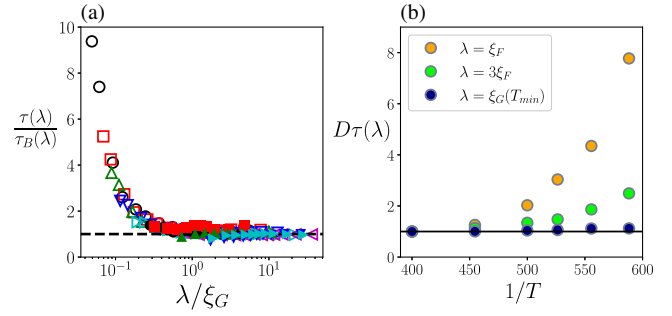

FIG. 4. (a) $\tau(\lambda)/\tau_B(\lambda)$ as a function of λ/ξ_G for both experiments at different area fractions (full symbols) and for simulations at different temperatures (empty symbols). (b) Simulations only: product $D\tau(\lambda)$ for three values of λ. Data have been rescaled for the values at the highest temperature.

Supplemental Material [29]). In Fourier space, the hallmarks of standard Brownian diffusion (both Fickian and Gaussian) are a pure exponential shape of the ISSF, i.e., $F_s(\lambda, t) = e^{-t/\tau_B(\lambda)}$ [57] and a wavelength-dependent relaxation time given by $\tau_B(\lambda) = [\lambda^2/(4\pi^2 D)]$. It is interesting to check how these features change and/or decouple when FnGD is present. In our systems, in fact, we confirm the occurrence of a simple exponential decay of the ISSF as far as $\tau(\lambda) > \tau_G$, where the characteristic relaxation time $\tau(\lambda)$ at a given wavelength is defined by $F_s[\lambda, \tau(\lambda)] \equiv 1/e$. For $\tau(\lambda) < \tau_G$, conversely, the observed non-Gaussian shape of the displacement distribution turns out to be mirrored into a stretched exponential ISSF decay, $e^{-\{t/[\tau(\lambda)]\}^{\beta(\lambda)}}$, with $\beta(\lambda) < 1$ (see Supplemental Material [29]). Hereafter, we will focus on the wavelength dependence of the relaxation time $\tau(\lambda)$ for wavelengths $\lambda \geq \xi_F$ only, i.e., where Fickian behavior is at play. Notice also that, since in both systems $\xi_F \simeq \lambda^*$ (where λ^* is the main peak of the structure factor), $\tau_\alpha \equiv \tau(\lambda^*)$ is around the lower boundary of the $\tau(\lambda)$ range investigated here.

Figure 4(a) shows $\tau(\lambda)/\tau_B(\lambda)$ vs λ/ξ_G for the entire set of simulations and experiments. We find all datasets to be compatible with a single master curve, which steeply decreases on increasing λ/ξ_G, and attains a unitary plateau, corresponding to standard-Brownian scaling, just around $\lambda/\xi_G = 1$. Notice that small λ/ξ_G values hint at a strong FnGD regime [58]: in fact, the range $\lambda/\xi_G < 0.5$ is covered by simulations only, whereas experimental data start close to the plateau.

It should be remarked that the behavior of τ/τ_B at small λ/ξ_G implies that the product $D\tau(\lambda)$ does depend on temperature. Such a Stokes-Einstein Breakdown (SEB) is commonly reported in systems approaching the glass transition, for wavelengths close to the first peak of the static structure factor, and is ascribed to the presence of marked DHs [59]. Figure 4(b) shows that, in our simulations, SEB is about a factor 8 at the lowest temperature and for $\lambda = \xi_F$, indicating that DHs are strongly at play when the dynamics is probed at the Fickian length scales.

Conversely, at a wavelength corresponding to the lowest-temperature Gaussian length, $\xi_G(T_{\min})$, the Stokes-Einstein behavior is fully recovered over the whole temperature range, suggesting that DHs are averaged out on this probe length. Overall, we can conclude that the recovery of *both* the standard-Brownian features in Fourier space is *solely* ruled by the Gaussian scale: the stretched exponentiality of ISSF and the λ dependence of its relaxation time remain coupled throughout FnGD.

In this Letter, we have highlighted the connection between two major issues in soft matter, namely, glass transition (a very long-standing problem) and the recently discovered FnGD. Glass-forming liquids are in fact a privileged stage to study FnGD, just because the microscopic dynamics and the emergence of dynamic heterogeneities have already been fairly well characterized in these systems.

It is apparent that the validation of the here-proposed scalings largely relies on the availability of long-time data for other glass formers, at many different values of the control parameter (temperature and concentration in our case) ruling the approach to glass transition. In general terms, it would be interesting to examine in detail the precursors of FnGD, which build up in the subdiffusive regime. In our glass-forming systems, strengthening of FnGD will correspond to deepening of subdiffusion. Such a phenomenology was also observed in recently introduced experimental model system of FnGD, with colloidal beads diffusing in a speckle field [60,61]. How much such a connection between precursors in the subdiffusive time window and FnGD is relevant on approaching glass transition is an intriguing open issue.

---

[*]Corresponding author.
raffaele.pastore@unina.it

[1] A. Einstein, Über die von der molekularkinetischen Theorie der Wärme geforderte Bewegung von in ruhenden Flüssigkeiten suspendierten Teilchen, Ann. Phys. (Berlin) **322**, 549 (1905).

[2] J.-P. Bouchaud and A. Georges, Anomalous diffusion in disordered media: Statistical mechanisms, models and physical applications, Phys. Rep. **195**, 127 (1990).

[3] Y. Meroz and I. M. Sokolov, A toolbox for determining subdiffusive mechanisms, Phys. Rep. **573**, 1 (2015).

[4] B. Wang, S. M. Anthony, S. C. Bae, and S. Granick, Anomalous yet Brownian, Proc. Natl. Acad. Sci. U.S.A. **106**, 15160 (2009).

[5] J. Guan, B. Wang, and S. Granick, Even hard-sphere colloidal suspensions display Fickian yet non-gaussian diffusion, ACS Nano **8**, 3331 (2014).

[6] J. Kim, C. Kim, and B. J. Sung, Simulation Study of Seemingly Fickian but Heterogeneous Dynamics of Two Dimensional Colloids, Phys. Rev. Lett. **110**, 047801 (2013).

[7] K. C. Leptos, J. S. Guasto, J. P. Gollub, A. I. Pesci, and R. E. Goldstein, Dynamics of Enhanced Tracer Diffusion in Suspensions of Swimming Eukaryotic Microorganisms, Phys. Rev. Lett. **103**, 198103 (2009).

[8] Z. Ghannad, Fickian yet non-Gaussian diffusion in two-dimensional Yukawa liquids, Phys. Rev. E **100**, 033211 (2019).

[9] T. Kwon, O.-S. Kwon, H.-J. Cha, and B. J. Sung, Stochastic and heterogeneous cancer cell migration: Experiment and theory, Sci. Rep. **9**, 1 (2019).

[10] K. He, F. Babaye Khorasani, S. T. Retterer, D. K. Thomas, J. C. Conrad, and R. Krishnamoorti, Diffusive dynamics of nanoparticles in arrays of nanoposts, ACS Nano **7**, 5122 (2013).

[11] R. Jeanneret, D. O. Pushkin, V. Kantsler, and M. Polin, Entrainment dominates the interaction of microalgae with micron-sized objects, Nat. Commun. **7**, 12518 (2016).

[12] F. Giavazzi, C. Malinverno, G. Scita, and R. Cerbino, Tracking-free determination of single-cell displacements and division rates in confluent monolayers, Front. Phys. **6**, 120 (2018).

[13] S. Nampoothiri, E. Orlandini, F. Seno, and F. Baldovin, Polymers critical point originates Brownian non-Gaussian diffusion, Phys. Rev. E **104**, L062501 (2021).

[14] S. Mora and Y. Pomeau, Tracking-Free Determination of Single-Cell Displacements and Division Rates in Confluent Monolayers, Phys. Rev. E **98**, 040101(R) (2018).

[15] M. V. Chubynsky and G. W. Slater, Diffusing Diffusivity: A Model for Anomalous, yet Brownian, Diffusion, Phys. Rev. Lett. **113**, 098302 (2014).

[16] A. V. Chechkin, F. Seno, R. Metzler, and I. M. Sokolov, Brownian yet Non-Gaussian Diffusion: From Superstatistics to Subordination of Diffusing Diffusivities, Phys. Rev. X **7**, 021002 (2017).

[17] E. Barkai and S. Burov, Packets of Diffusing Particles Exhibit Universal Exponential Tails, Phys. Rev. Lett. **124**, 060603 (2020).

[18] V. Sposini, A. V. Chechkin, F. Seno, G. Pagnini, and R. Metzler, Random diffusivity from stochastic equations: comparison of two models for Brownian yet non-Gaussian diffusion, New J. Phys. **20**, 043044 (2018).

[19] B. Wang, J. Kuo, S. C. Bae, and S. Granick, When Brownian diffusion is not Gaussian, Nat. Mater. **11**, 481 (2012).

[20] R. Metzler, Gaussianity fair: The riddle of anomalous yet non-gaussian diffusion, Biophys. J. **112**, 413 (2017).

[21] P. Chaudhuri, L. Berthier, and W. Kob, Universal Nature of Particle Displacements close to Glass and Jamming Transitions, Phys. Rev. Lett. **99**, 060604 (2007).

[22] R. Pastore, A. Coniglio, and M. P. Ciamarra, From cage-jump motion to macroscopic diffusion in supercooled liquids, Soft Matter **10**, 5724 (2014).

[23] E. R. Weeks, J. C. Crocker, A. C. Levitt, A. Schofield, and D. A. Weitz, Three-dimensional direct imaging of structural relaxation near the colloidal glass transition, Science **287**, 627 (2000).

[24] L. Berthier, G. Biroli, J.-P. Bouchaud, and R. L. Jack, *Dynamical Heterogeneities in Glasses, Colloids, and Granular Media* (Oxford University Press, Oxford, 2011), Vol. 150, p. 68.

[25] N. Lačević, F. W. Starr, T. Schrøder, and S. Glotzer, Spatially heterogeneous dynamics investigated via a time-dependent four-point density correlation function, J. Chem. Phys. **119**, 7372 (2003).

[26] R. Das, C. Dasgupta, and S. Karmakar, Time scales of Fickian diffusion and the lifetime of dynamic heterogeneity, Front. Phys. **8**, 210 (2020).

[27] Just a few days before the submission of this Letter, a numerical study was published on one of the topics addressed in this Letter, namely, the time-dependence of the decay-length of the displacement distribution tails [28]. Our result on this aspect is at variance with the one reported in that paper.

[28] J. M. Miotto, S. Pigolotti, A. V. Chechkin, and S. Roldán-Vargas, Length Scales in Brownian yet Non-Gaussian Dynamics, Phys. Rev. X **11**, 031002 (2021).

[29] See Supplemental Material at http://link.aps.org/supplemental/10.1103/PhysRevLett.128.168001, for details on experiments and simulations and for additional results, which includes Refs. [29–46].

[30] J. C. Crocker and D. G. Grier, Methods of digital video microscopy for colloidal studies, J. Colloid Interface Sci. **179**, 298 (1996).

[31] E. Jones, T. Oliphant, and P. Peterson, http://www.scipy.org (2014).

[32] F. Pérez and B. E. Granger, IPython: A system for interactive scientific computing, Comput. Sci. Eng. **9**, 21 (2007).

[33] S. Plimpton, Fast parallel algorithms for short-range molecular dynamics, J. Comput. Phys. **117**, 1 (1995).

[34] W. Shinoda, M. Shiga, and M. Mikami, Rapid estimation of elastic constants by molecular dynamics simulation under constant stress, Phys. Rev. B **69**, 134103 (2004).

[35] M. Schmiedeberg, J. Roth, and H. Stark, Brownian particles in random and quasicrystalline potentials: How they approach the equilibrium, Eur. Phys. J. E **24**, 367 (2007).

[36] M. Fuchs, W. Götze, and M. R. Mayr, Asymptotic laws for tagged-particle motion in glassy systems, Phys. Rev. E **58**, 3384 (1998).

[37] P. Charbonneau, Y. Jin, G. Parisi, and F. Zamponi, Hopping and the Stokes–Einstein relation breakdown in simple glass formers, Proc. Natl. Acad. Sci. U.S.A. **111**, 15025 (2014).

[38] W. Kob and H. C. Andersen, Concentrated suspensions of Brownian beads in water: dynamic heterogeneities through a simple experimental technique, Phys. Rev. E **51**, 4626 (1995).

[39] R. Pastore, M. Caggioni, D. Larobina, L. S. Amato, and F. Greco, Concentrated suspensions of Brownian beads in water: Dynamic heterogeneities through a simple experimental technique, Sci. China Phys. Mech. Astron. **62**, 107006 (2019).

[40] J. Helfferich, J. Brisch, H. Meyer, O. Benzerara, F. Ziebert, J. Farago, and J. Baschnagel, Continuous-time random-walk approach to supercooled liquids: Self-part of the van Hove function and related quantities, Eur. Phys. J. E **41**, 71 (2018).

[41] M. Hurley and P. Harrowell, Non-Gaussian behavior and the dynamical complexity of particle motion in a dense two-dimensional liquid, J. Chem. Phys. **105**, 10521 (1996).

[42] T. Odagaki and Y. Hiwatari, Stochastic model for the glass transition of simple classical liquids, Phys. Rev. A **41**, 929 (1990).

[43] C. F. E. Schroer and A. Heuer, Anomalous Diffusion of Driven Particles in Supercooled Liquids, Phys. Rev. Lett. **110**, 067801 (2013).

[44] T. Odagaki, J. Matsui, and Y. Hiwatari, Trapping diffusion model for glass transition and slow dynamics in supercooled liquids, Physica (Amsterdam) **204A**, 464 (1994).

[45] E. Flenner and G. Szamel, Relaxation in a glassy binary mixture: Comparison of the mode-coupling theory to a Brownian dynamics simulation, Phys. Rev. E **72**, 031508 (2005).

[46] D. R. Reichman and P. Charbonneau, Mode-coupling theory, J. Stat. Mech. Theory Exp. **2005**, P05013 (2005).

[47] W. Götze, *Complex Dynamics of Glass-Forming Liquids: A Mode-Coupling Theory* (OUP, Oxford, 2008), Vol. 143.

[48] K. H. Nagamanasa, S. Gokhale, A. Sood, and R. Ganapathy, Direct measurements of growing amorphous order and non-monotonic dynamic correlations in a colloidal glass-former, Nat. Phys. **11**, 403 (2015).

[49] S. Vivek, C. P. Kelleher, P. M. Chaikin, and E. R. Weeks, Long-wavelength fluctuations and the glass transition in two dimensions and three dimensions, Proc. Natl. Acad. Sci. U.S.A. **114**, 1850 (2017).

[50] S. Gokhale, K. H. Nagamanasa, R. Ganapathy, and A. Sood, Growing dynamical facilitation on approaching the random pinning colloidal glass transition, Nat. Commun. **5**, 4685 (2014).

[51] The recorded experimental trajectories are available at the corresponding author website: http://rpastore.altervista.org/Repository/.

[52] D. N. Perera and P. Harrowell, Stability and structure of a supercooled liquid mixture in two dimensions, Phys. Rev. E **59**, 5721 (1999).

[53] R. Pastore, G. Pesce, A. Sasso, and M. P. Ciamarra, Many facets of intermittent dynamics in colloidal and molecular glasses, Colloids Surf. A **532**, 87 (2017).

[54] $p(x, t)$ is computed over both the x and y component of displacements, since systems are isotropic.

[55] At high temperature the recovery of Gaussianity is relatively rapid and exponential tails become quickly limited to a small X range.

[56] Deviations from the indicated power law are found in experiments, for $t < \tau_F$. (see Supplemental Material [29]).

[57] A. L. Thorneywork, D. G. Aarts, J. Horbach, and R. P. Dullens, On the Gaussian approximation in colloidal hard sphere fluids , Soft Matter **12**, 4129 (2016).

[58] Existence of small values λ/ξ_G implies $\xi_G \gg \xi_F$.

[59] A. Cavagna, Supercooled liquids for pedestrians, Phys. Rep. **476**, 51 (2009).

[60] R. Pastore, A. Ciarlo, G. Pesce, F. Greco, and A. Sasso, Rapid Fickian Yet Non-Gaussian Diffusion after Sub-diffusion, Phys. Rev. Lett. **126**, 158003 (2021).

[61] R. Pastore, A. Ciarlo, G. Pesce, A. Sasso, and F. Greco, A model-system of Fickian yet non-Gaussian diffusion: Light patterns in place of complex matter, Soft Matter **18**, 351 (2022).